



## OPEN Effects of electrode placement on electrical stimulation for wound healing

Suhyeok Kim<sup>1,4</sup>, Donghun Kang<sup>2,4</sup>, Youngseok Choi<sup>3</sup>, Jeyeon Lee<sup>2</sup>, Jongshill Lee<sup>2</sup>, In Young Kim<sup>2</sup>✉ & Eunyoung Park<sup>1</sup>✉

Effective wound healing is directly linked to survival. Long-term unhealed wounds impair quality of life and incur significant costs. Electrical stimulation (ES) influences wound healing by modulating signals that regulate cell proliferation, migration, and immune response. In ES treatment, the placement of electrodes is a critical factor, as it impacts the environmental conditions and cell polarity essential for wound healing. This study analyzed the effects of various electrode placements to identify the optimal setup for accelerating wound healing. The optimized electrode placement enhanced wound healing in a rat model of full-thickness skin defect over 17 days, and the electrical field (EF) was analyzed using simulations. In-vivo, the optimized electrode placement achieved a 16.7% reduction in wound area compared to the control group. In simulation, a forward vector of the EF from the optimized electrode placement was observed. The findings suggest that optimizing the electrode placement for ES is beneficial to wound healing.

A wound is defined as an injury or disorder of the skin structure, extending from the epithelium to the deep tissues and organs<sup>1</sup>. The natural wound healing process initiates with the occurrence of a wound and typically spans 4 to 6 weeks, encompassing phases of coagulation and hemostasis, inflammation, proliferation, and remodeling<sup>2-5</sup>. Factors, whether local, systemic, or general, can impede wound healing<sup>6,7</sup>. Chronic wounds are defined as those that fail to restore anatomic and functional integrity within 3 months<sup>8</sup>. Factors such as aging and diabetes can lead to delayed wound healing, which may progress to chronic wounds. Chronic wounds can lead to increased healthcare costs due to extended healing periods, infections, mutilations, complications, and reduced quality of life. In the United States, 6.5 million patients annually incur over US\$25 billion in expenses related to chronic wounds<sup>9</sup>. Furthermore, chronic wounds are vulnerable to exogenous pathogens, such as sepsis<sup>10</sup>. Additionally, diabetic foot ulcers (DFUs), which are a complication of diabetes, can lead to amputations and high mortality rates<sup>11</sup>. Consequently, quality of life significantly declines. Addressing these issues by shortening the healing period and preventing chronic wounds can reduce both economic costs and the prevalence of complications, ultimately enhancing quality of life. Therefore, accelerating wound healing is crucial both to shorten the healing period and to prevent the development of chronic wounds.

A variety of strategies have been studied to accelerate wound healing and to prevent and treat chronic wounds. Treatments such as ultrasound, compression bandage, cell transplantation, dressings, infrared, hyperbaric oxygen therapy, and ES have utilized for wound healing<sup>1,12-21</sup>. Several experimental approaches have proven effective in accelerating wound healing. However, these treatments present challenges such as high treatment and development costs, prolonged healing duration, and patient stress. ES has garnered attention as a generally safe, cost effective, and efficient treatment for chronic wounds caused by various factors<sup>22-26</sup>.

ES treatment utilizes the biological principles of wound healing. The physiological factors of wound healing are known as trans-epithelial potential (TEP), which ranges from 10 to 60 mV across the epidermis<sup>27,28</sup>. Wound formation disrupts the highly resistive epithelium, thereby creating a pathway of lower resistance. This disruption leads to a loss of TEP and ion movements, resulting in a potential difference that directs towards the wound site and induces endogenous EF<sup>29-31</sup>. Cell migration for wound healing is induced by endogenous EF<sup>32,33</sup>. ES generates exogenous EF that imitates endogenous EF and promotes cell migration. Proper ES application accelerates wound healing significantly, as various studies have shown the effectiveness of ES in accelerating the healing process especially hard-to-heal wounds<sup>34-36</sup>. However, specific parameters must be considered when applying ES. The first is the waveform of stimulation. Variations in stimulation waveform have been shown

<sup>1</sup>Department of Biomedical Engineering, Soonchunhyang University, Asan, Korea. <sup>2</sup>Department of Biomedical Engineering, Hanyang University, Seoul, Korea. <sup>3</sup> Department of Electronic Engineering, Hanyang University, Seoul, Korea. <sup>4</sup>Suhyeok Kim and Donghun Kang have contributed equally to this work. ✉email: iykim@hanyang.ac.kr; ek.park@sch.ac.kr

to impact effectiveness; high voltage pulse current (HVPC) is most effective in reducing wound size<sup>37,38</sup>. The second parameter is the placement of electrodes. Electrode placement affect the formation of exogenous EF<sup>39</sup>. In wound healing, the formation of exogenous EF, including its direction and penetration depth, is crucial due to the different polarities of cells predominantly located in the dermis layers<sup>40,41</sup>. Inappropriate direction and penetration depth of EF can hinder wound healing and potentially lead to chronic wounds. Previous studies have employed four methods of electrode placement. The first method involves placing ground and active electrodes on opposite sides of the wound<sup>42–44</sup>. The second method positions an active electrode on the wound and a ground electrode adjacent to it<sup>45,46</sup>. The third method places an active electrode on the wound and ground electrodes on both side of the wound<sup>34</sup>. The remaining methods utilize a ring-shaped electrode that positions an active electrode on the wound and a ground electrode around the wound<sup>13,47</sup>. Several studies that adopted the first three placements failed to explain their choice or assess the impact of these placements<sup>34,42–46</sup>. These placements are not expected to facilitate optimal wound healing. In silico studies suggest that a ring-shaped electrode configuration most closely mimics endogenous EF<sup>48</sup>. However, there are challenges associated with applying ring-shaped electrodes to wounds of varying sizes and shapes due to the fixed size of electrode. In a study conducted by Song, Joseph W., et al., an electrode for wound healing with a diameter of 8 mm was developed<sup>13</sup>. However, this electrode was unable to apply to wounds exceeding 8 mm in diameter. In summary, while several studies have investigated the effects of stimulation waveforms, research on the impact of electrode placement is lacking. Moreover, the application of electrode placements is not standardized, limiting their compatibility with various wound types.

In this study, we report on the effect of wound healing based on various electrode placements. To address the limitations of conventional wound treatments, such as electrode placements with unclear principles and electrodes of a fixed size, we developed an adaptable electrode placement without a fixed shape. The groups were categorized based on several criteria, and the effects of EF on wound healing were quantified and compared across multiple experimental settings. In this experiment, proliferation and remodeling were promoted after 7 days of hemostasis and inflammation<sup>49</sup>. In-vivo animal models were employed to examine the impacts of varying electrode numbers and positions. Physiological analysis was conducted on full thickness wound models located on the dorsal area of rats to investigate collagen secretion, epithelium layer thickness, and wound size. Simulation analysis evaluated the formation of EFs and electric currents using COMSOL Multiphysics software. The study investigated the direction, density, and penetration depth of EFs and electric currents. Different electrode placements resulted in varying rates of wound healing and the formation of EFs. The correlation between in-vivo and in silico results was analyzed to optimize electrode placement in ES for wound healing. To address the limitations of current wound treatment methods, including electrode placement with unclear principles and fixed-size electrodes, we developed a versatile electrode placement. The groups were categorized based on multiple criteria, and the effects on wound healing were evaluated across various experimental settings. This study aims to confirm the impact of electrode placement on wound healing and to suggest guidelines for applying ES treatment to diverse types of wounds.

## Methods

### Animal use

The in-vivo study was approved by the Institutional Animal Care and Use Committee of Soonchunhyang University with an approval number SCH23-0028. All animal experiments adhered to international guidelines for the care and use of laboratory animals and are reported under the ARRIVE guidelines.

### Properties of electrical stimulation

A custom-built high voltage pulsed current (HVPC) stimulator was developed for this study. The overall architecture of the stimulator is summarized in a block diagram (Fig. 1a). The device is capable of delivering pulsed stimulation with a maximum peak voltage of 60 V. Stimulation parameters, including pulse width, frequency, and amplitude, are controlled via a Bluetooth-enabled interface developed in C#.

The electrical performance and safety of the stimulator were validated by an officially certified testing agency (Osong Medical Innovation Foundation, Korea), in accordance with medical device standards for low-frequency electrical stimulators. The results of the electrical safety test (Test report number: MDDC-T20-BM185) confirmed stable and accurate output characteristics, with a pulse width error of  $2.22 \pm 1.69\%$ , a frequency error of  $0.10 \pm 0.00\%$ , and a peak voltage error of  $-5.46 \pm 3.60\%$ .

HVPC, which was used in this study, features a monophasic twin-peak waveform and has demonstrated efficacy in wound healing compared to other waveforms, such as direct current (DC) or alternating current (AC)<sup>37,38</sup>. The stimulation parameters were 50 V amplitude, 100 Hz frequency, and 1% duty ratio (Fig. 1b). During the measurements, the size and placement of electrodes matched those used in the in-vivo experiments.

### Sample size

In accordance with the 3Rs principles (Replacement, Reduction, and Refinement), the number of animals was minimized. The size of group was based on previous studies on rat model<sup>50</sup>. A total of 32 rats were randomly divided into four groups. The animals were excluded if the animal died prematurely, preventing the collection of histological data. Results were obtained from the following sample sizes: Control (n = 8), Group 1 (n = 7), Group 2 (n = 8), Group 3 (n = 7).

### Wound model of full-thickness skin defect

For the full-thickness skin defect model, Sprague–Dawley rats (KOATECH, Korea) weighing between 240 and 260 g were utilized after a 1-week acclimatization period and were housed with free access to food and water and 12 h/12 h regular day and night. All procedures were conducted under anesthesia with isoflurane in oxygen.

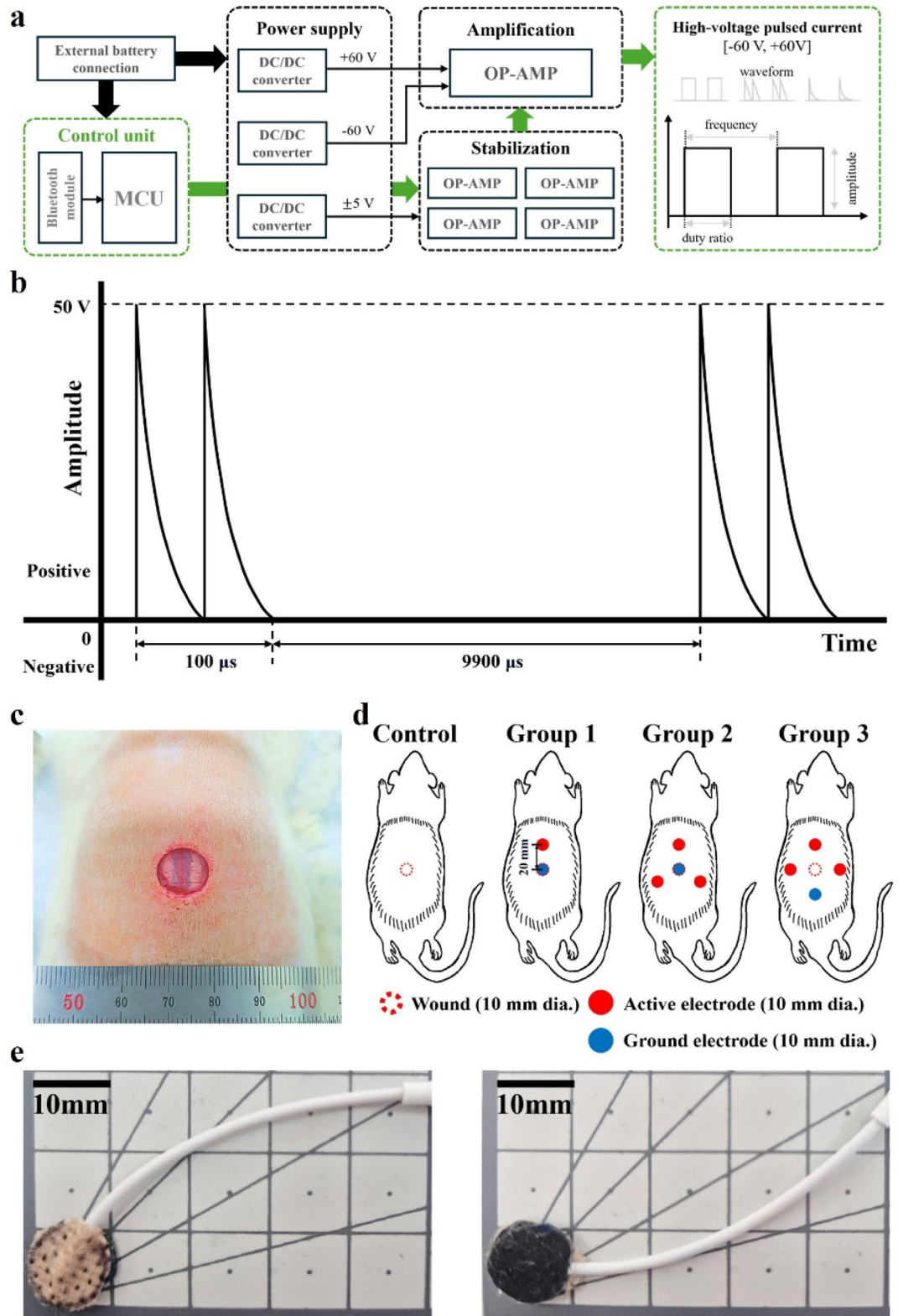


**Fig. 1.** (a) A custom-built HVPC stimulator block diagram (b) Stimulation waveform parameter of ES for wound healing. (c) Wound model of full-thickness skin defect on the dorsal surface of rat. (d) Group categorization by electrode placement. (e) Front (left) and back (right) images of the modified electrode.

After hair removal and disinfection with alcohol gauze, a full-thickness wound was created on the dorsal surface of the rats using a biopsy punch (Fig. 1c). The wound had a diameter of 10 mm. Apart from the control group, three additional groups (1, 2, and 3) received ES treatment (Fig. 1d). The control group was untreated, and no electrodes were placed. Group 1 received treatment with one ground electrode and one active electrode, with the ground electrode placed over the wound and the active electrode placed around the wound. The centers of the two electrodes were spaced 20 mm apart. Groups 2 and 3 received treatments involving one ground electrode and three active electrodes. In Group 2, the ground electrode was placed over the wound, and the active electrodes were placed around the wound. The centers of the ground electrode and the active electrode were spaced 20 mm apart and each of three active electrodes were equidistant from neighboring active electrodes. In Group 3, one ground electrode and three active electrodes were placed around the wound. The centers of all electrodes and the wound were spaced 20 mm apart, with each electrode equidistant from its neighbors. Electrodes (VTX5050, Axelgaard Manufacturing Co., Ltd., California), which are commercially available and validated for safety, were used with a circular design and a reduced diameter of 10 mm (Fig. 1e). During each stimulation session, a saline-soaked gauze was placed over the wound. The positions of the electrodes remained consistent throughout the study and were secured with medical tape. HVPC stimulation was applied for 30 min per day<sup>51</sup>. During stimulation, the rats were kept anesthetized, and the study spanned 17 days.

The experiment began on day 0, and the wound area was photographed daily using a digital camera. Wound size was quantified with the ImageJ 1.54 g software (<https://wsr.imagej.net/ij/>), and the percentage of wound area was calculated using Eq. (1), where N is the date of the experiment.

$$\text{Wound area} = (\text{Day N wound size}) / (\text{Day 0 wound size}) \times 100(\%) \quad (1)$$

## Histology

After 17 days, animals were anesthetized with isoflurane and euthanized using carbon dioxide. Subsequently, tissue samples were collected from around the wound on the dorsal surface. These samples were fixed in 4% paraformaldehyde and embedded in paraffin blocks. Once sliced, these sections underwent deparaffinization and dehydration using Xylene and EtOH. The slices were then stained with hematoxylin and eosin (H&E) for microscopic examination. The epithelium and granulation tissue gaps were analyzed.

## Statistical analysis

Data analysis was performed by SPSS29.0.2.0 statistical software (<https://www.ibm.com/products/spss>). Results are presented as mean  $\pm$  standard error of the mean (SEM). Statistical analyses were conducted using the Kruskal Wallis test. A p-value < 0.05 was considered statistically significant. As a non-parametric test, it was applied without correction for multiple comparisons.

## Simulation analysis

### Wound and electrode model

We constructed a three-dimensional finite element model of wound and electrode using COMSOL Multiphysics 5.5 (<https://www.comsol.com/>). To develop a wound model, a cylindrical skin model was created with a total thickness of 13.514 mm and a diameter of 120 mm. This skin layer included the stratum corneum, epidermis, dermis, subcutis fat, and muscle, with thicknesses of 0.014 mm, 0.3 mm, 2.2 mm, 3 mm, 3 mm, and 5 mm, respectively. A wound with a depth of 4 mm and a diameter of 10 mm was simulated at the center of the skin model, penetrating to the middle of the subcutis layer. The wound was filled with phosphate-buffered saline (PBS), which exhibits good electrical conductivity, drawing upon prior research<sup>48</sup> that established the wound model. The geometries of the skin and wound models are displayed in the upper section of Fig. 2a; the lower

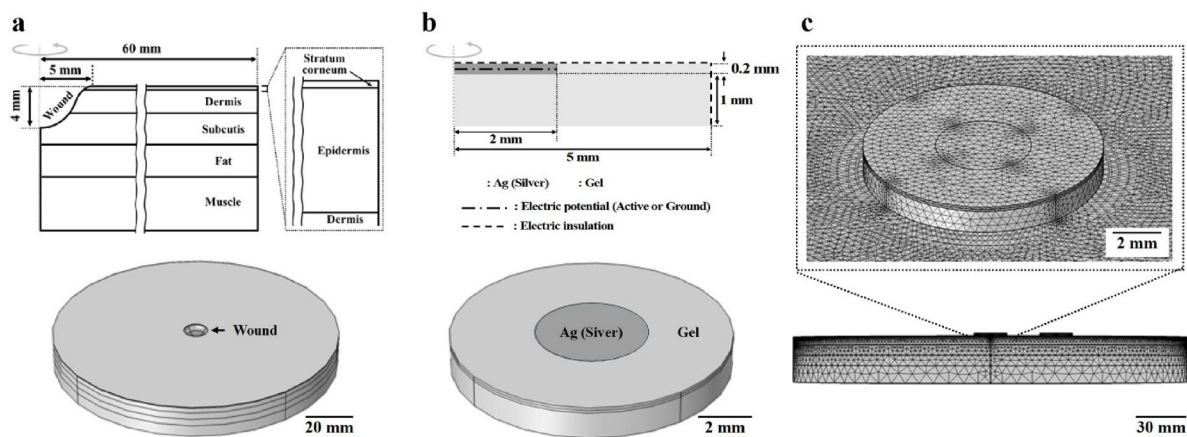


**Fig. 2.** Geometry and three-dimensional finite element model in COMSOL Multiphysics. (a) Geometry and finite element model of the skin and the wound. (b) Geometry and finite element model of the electrode model. (c) Constructed mesh of Group 1's finite element model.

	Thickness [mm]	Conductivity [ $\sigma$ in S/m]
Ag (Silver)	–	6.16E+06 <sup>53</sup>
Gel	–	1 <sup>55</sup>
PBS	–	1.4 <sup>48</sup>
Air	–	1.00E-13 <sup>52</sup>
Stratum corneum	0.014 <sup>48</sup>	2.00E-06 <sup>48</sup>
Epidermis	0.3 <sup>48</sup>	0.026 <sup>48</sup>
Dermis	2.2 <sup>48</sup>	0.222 <sup>48</sup>
Subcutis	3 <sup>48</sup>	0.08 <sup>48</sup>
Fat	3	2.50E-02 <sup>54</sup>
Muscle	5	5.00E-01 <sup>54</sup>

**Table 1.** Electrical properties of materials used in the wound and electrode model.

	Group 1	Group 2	Group 3
Tetrahedral elements	7,218,596	7,309,296	7,218,583
Triangular elements	633,203	647,723	647,853
Edge elements	5,933	7,053	7,129
Vertex elements	109	165	169
Minimum elements quality	4.33E-04	1.66E-04	4.33E-04
Average elements quality	0.6163	0.6157	0.6149
Element volume ratio	3.97E-12	1.76E-12	1.24E-12
Mesh volume	8.0E09 mm <sup>3</sup>	8.0E09 mm <sup>3</sup>	8.0E09 mm <sup>3</sup>

**Table 2.** Statistical data of mesh for each electrode placement. The unit of measurement for elements is numbers.

section details the finite element model of the skin and wound as developed in COMSOL Multiphysics. The electrode was designed as a cylindrical shape with a height of 1.2 mm and a diameter of 10 mm, composed of Ag (Silver) as substrate of the electrode and conductive gel, with an Ag layer having a height of 0.2 mm and a diameter of 4 mm positioned at the upper center of the gel. Figures in the upper and lower sections of Fig. 2b depict the geometry and finite element model of the electrode. The boundary conditions of the electrodes are indicated by dotted lines in the upper section of Fig. 2b. The electric potential of the electrodes (either active or ground) was applied to the horizontal mid-plane of the Ag component, located 0.1 mm below the top surface of the electrode. Electric insulation conditions were applied to all external surfaces of the electrode except for the bottom surface in contact with the skin. This approach differs from the conventional method, in which the electrode volume is excluded from the modeling domain and a fixed voltage is imposed only on the electrode surface to ensure numerical stability and computational efficiency. However, due to the high conductivity of silver, the potential was uniformly distributed across the Ag surface, resulting in numerically equivalent behavior to the conventional fixed-surface voltage condition. Validation of the potential distribution confirmed that a nearly constant potential was maintained across the entire Ag layer, and the corresponding voltage distribution map is provided in Supplementary Figure S1. A cube-shaped air domain with a length of 2000 mm, which was filled with air, was constructed around the wound model. For the cube-shaped air domain surrounding the skin model, electric insulation boundary conditions were applied to all external faces to prevent current leakage. The electrical properties of the materials used in the wound and electrode model are summarized in Table 1<sup>48,52–55</sup>.

We constructed our model based on several assumptions. Initially, we assumed that the wound and electrode models were composed of homogeneous isotropic materials, using materials with constant electrical conductivity. Additionally, the wound model omitted several skin tissue components, such as sweat glands, lymph vessels, and blood vessels (arteries, veins, capillaries). Moreover, cellular processes such as the Na<sup>+</sup>/K<sup>+</sup> pump and different cell types, including keratinocyte and macrophage, were not considered.

The electrode placement and the distance between the electrodes and the wound were set to match the in-vivo experimental conditions described in Fig. 1c. The mesh statistics of the finite element model are presented in Table 2. Figure 2c illustrates the mesh formed by the electrode placement for group 1, the lower section shows the side view of the constructed model, while the upper section depicts the mesh of the ground electrode placed on the wound.

#### Simulation setting for each electrode placement

The potential was set in Ag, as shown in Fig. 2b, to conduct the simulation of each electrode placement of ES. The potential of the ground electrode was set to ground, and the potential of the active electrode was set to the root mean square voltage ( $V_{rms}$ : 2.887 V), calculated by Eq. (2), where  $T$  is period,  $V(t)$  is potential for one period of the stimulation waveform described in Fig. 2a.

$$V_{\text{rms}} = \sqrt{\frac{1}{T} \int_0^T V(t)^2 dt} \quad (2)$$

We performed simulations only for exogenous EF and excluded the effects of endogenous EF to clarify ES-induced EF and electric current flow. Moreover, the constructed model solved the Poisson equation ( $\nabla \cdot (\sigma \nabla V) = 0$ ;  $\sigma =$  conductivity,  $V =$  potential) under the quasi-static assumption.

Under the described conditions, we conducted several simulation analyses. We assessed the current density in the longitudinal section across the wound and the ground electrode for each electrode placement to determine how ES-induced electric current flow varied across each skin layer and wound. Furthermore, we evaluated the skin layer that exhibited the highest current density by ES, extracting the maximum, minimum, and average current density values from each skin layer. These values were then used to evaluate the penetration depth of electric current for each electrode placement.

The dermis is a skin layer that contains various wound-related cells including macrophages, fibroblasts, and neutrophils, and plays an essential role throughout the healing phases (e.g., inflammatory, proliferative)<sup>40,41</sup>. Consequently, we explored the current density and EF resulting from ES in the cross section at the horizontal center of the dermis layer (1.1 mm above the interface between subcutis and dermis or 1.414 mm depth from the skin surface). Additionally, assuming that the size of the wound decreases due to ES, we assessed the EF of the dermis when the wound diameter was 10 mm, 8 mm, and 4 mm.

## Results

### In-vivo effect of electrode placement on wound healing

#### Wound area analysis

To evaluate the impact of electrode placement on wound healing, an in-vivo experiment utilized a wound model of full-thickness skin defect. Figure 3a presents representative images of wound closure at various time points across different groups. By day 7, there was no significant closure of the wounds in both control and experimental groups. By day 10, the wound areas began to decrease in the experimental groups. Subsequently, the wound areas gradually decreased over time in both the control and experimental groups. The wound area ratios were calculated based on the wound area at different time points, as shown in Fig. 3b. By day 15, the wound area ratio for group 3 was  $17.8 \pm 2.4\%$ . This group showed a statistically significant decrease compared to the control group, which was  $32.2 \pm 3.8\%$ . By day 17, the wound area ratios for the control group, group 1, and group 2 were  $25.6 \pm 3.5\%$ ,  $15.9 \pm 2.3\%$ , and  $17.5 \pm 3.0\%$  respectively. In contrast, the wound area ratio for group 3 significantly decreased, reaching  $8.9 \pm 0.7\%$ . Figure 3c illustrates the progression of the wound tracing analysis over time. By day 17, wounds in group 3 had nearly closed, whereas those in the control group, group 1, and group 2 were still clearly visible.

#### Histology analysis

Histological analysis was utilized to assess the influence of electrode placement on wound healing in ES treatment. Figure 4a presents the H&E staining results of wounds sampled after 17 days, where red arrows indicate the wound edge, showing re-epithelialization level, and black arrows denote granulation tissue, showing cell proliferation level. By examining the gap of epithelium and granulation tissue, one can histologically evaluate the impact of electrode placement on wound healing in ES treatment. Figure 4a and b demonstrate that the epithelium gap of group 3 ( $2.5 \pm 0.3$  mm) was statistically significantly smaller than that of control group ( $4.2 \pm 0.4$  mm), group 1 ( $3.9 \pm 0.6$  mm), and group 2 ( $3.9 \pm 0.5$  mm). Granulation tissue appeared in both control and experimental groups in Fig. 4a. In group 3 ( $2.9 \pm 0.3$  mm), the size of the granulation tissue gap, signaling the end of the proliferation phase, was statistically significantly the smallest in both Fig. 4a and c. The sizes of the granulation tissue gaps in the control group, group 1, and group 2 were  $5.1 \pm 0.5$  mm,  $4.9 \pm 0.6$  mm, and  $4.3 \pm 0.4$  mm, respectively.

The wound healing rate and H&E staining results from in-vivo experiments demonstrated that the electrode placement using four electrodes placed around the wound (group 3) significantly enhanced wound healing compared to the other groups (group 1, group 2).

### Simulation analysis

We conducted a simulation analysis to compare and assess the electric current and EF generated by different electrode placements. These quantitative simulation results were obtained several assumptions, including homogeneous isotropic material properties, simplified tissue composition, and cellular processes. Accordingly, the results are intended to provide qualitative insights rather than precise quantitative predictions.

We analyzed how the electric current flow varied across the skin layers and wound regions based on the current density in the longitudinal section across the wound and the ground electrode for each electrode placement. In group 2, where an electrode and the wound region displayed the highest current density (maximum value of wound surface =  $3.1092$  A/m<sup>2</sup>). Group 1 was lower than group 2 but exhibited a high current density (maximum value of wound surface =  $1.0637$  A/m<sup>2</sup>). In the wound region, group 3 demonstrated the lowest current density (maximum value of wound surface =  $0.063636$  A/m<sup>2</sup>). Placing the electrode on the wound (group 1, group 2) induced a higher current density than when the electrode was not placed on the wound (group 3). Moreover, group 2, with a greater number of electrodes, showed a higher induced current density than group 1. This trend remained consistent across all skin layers, particularly within the dermis.

We examined the current density for each skin layer to predict the current induced by ES in each layer (Table 3). We confirmed that, although the average current density of each skin layer varied depending on electrode placement, the dermis consistently showed the highest values for all electrode placements. When analyzing the

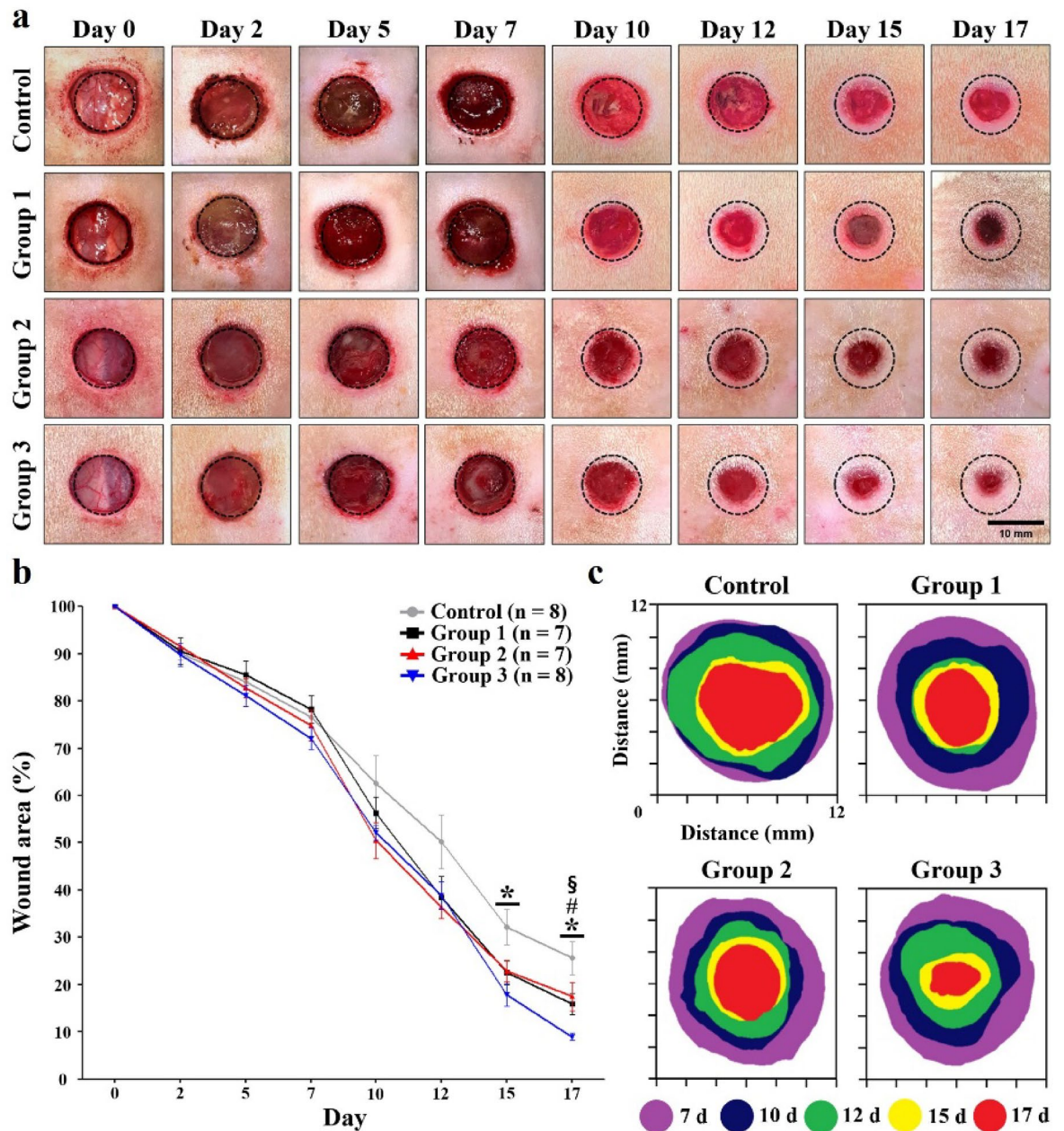


**Fig. 3.** In-vivo wound healing effect of electrode placement in ES. (a) Representative images of wounds on the dorsal of rat treated by ES of different area placements. (b) Quantification of wound area ratios within 17 days, control (gray), group 1 (black), group 2 (red), group 3 (blue). \* $p < 0.05$  between the control group and group 3, # $p < 0.05$  between group 1 and group 3, \$ $p < 0.05$  between group 2 and group 3 by Kruskal Wallis test. (c) Wound tracing analysis at different time points in different groups.

current density in the dermis across different electrode placements, both the maximum and average values were highest in group 2, followed by group 1, and then group 3 (maximum:  $2.10E+00$  A/m<sup>2</sup>,  $8.04E-01$  A/m<sup>2</sup>,  $4.79E-01$  A/m<sup>2</sup>; average:  $5.11E-02$  A/m<sup>2</sup>,  $2.28E-02$  A/m<sup>2</sup>,  $1.93E-02$  A/m<sup>2</sup>, respectively). Thus, ES induced the highest current density in the dermis layer regardless of the electrode placement, with group 2 showing the highest current density compared to the other groups.

We investigated the current density (Fig. 5a) induced by ES in a cross section of the dermis layer. The maximum current density and EF showed highest values in group 2, followed by group 1, and group 3 (current density:  $1.52097$  A/m<sup>2</sup>,  $0.52494$  A/m<sup>2</sup>,  $0.25049$  A/m<sup>2</sup>, respectively). We also studied the EF at locations across the wound and at the ground electrode for wound diameters of 10 mm, 8 mm, and 2 mm, and assessed the EF strength in the dermis relative to the wound diameter (Fig. 5b). The EF strength near the wound area was higher in group 2, followed by group 1, and group 3, independent of the wound diameter. Moreover, we observed that, for all electrode placements, the EF strength generally increased as the wound size decreased. Notably, group 3

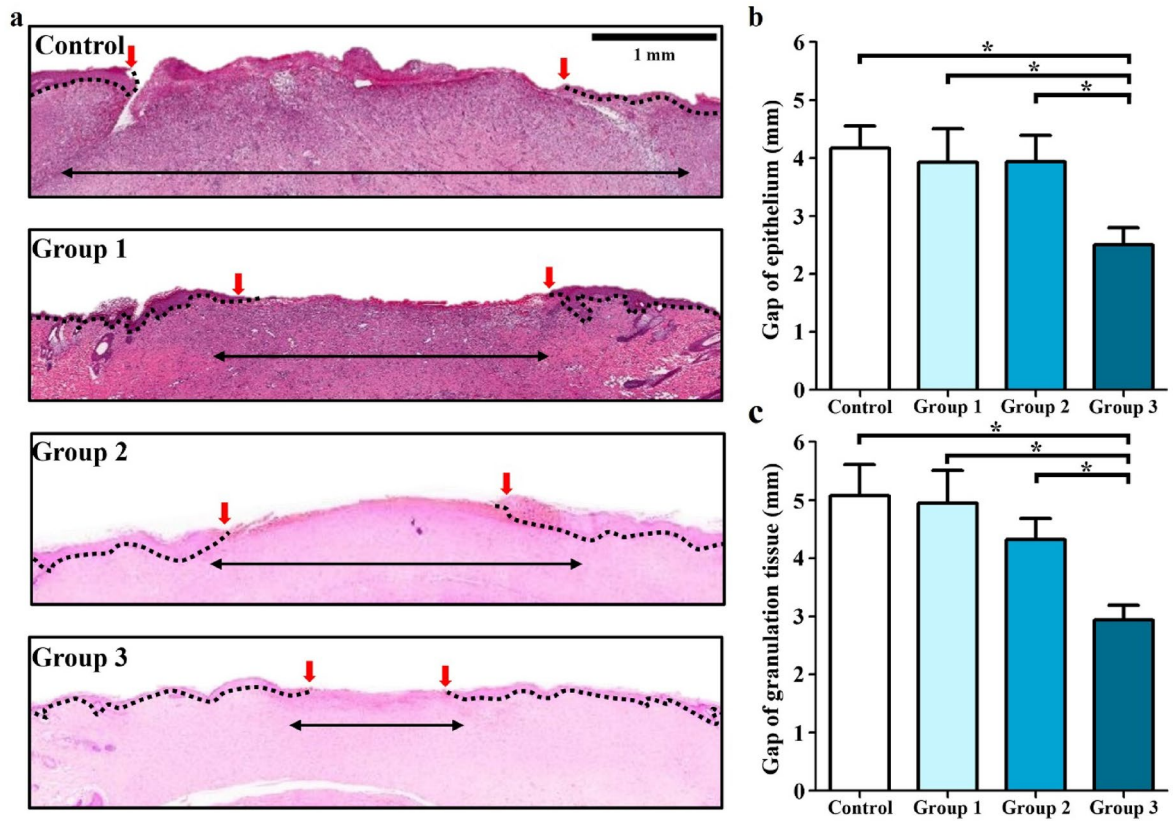


**Fig. 4.** H&E wound healing effect of electrode placement in ES treatment (a) Representative images of H&E staining of skin tissue after 17 days. Red arrows indicate the wound edge. Black arrows indicate granulation tissue. (b) epithelium and (c) granulation tissue gap based on H&E. \* $p < 0.05$  by Kruskal Wallis test.

Layer	Current density [A/m <sup>2</sup> ]								
	Group 1			Group 2			Group 3		
Value	Min	Max	Avg	Min	Max	Avg	Min	Max	Avg
Corneum	2.33E-13	7.74E-01	2.97E-03	1.00E-12	7.96E-01	8.84E-03	5.43E-13	5.54E-01	4.46E-03
Epidermis	2.53E-09	5.92E-01	5.47E-03	1.16E-08	8.70E-01	1.43E-02	5.08E-09	4.28E-01	6.39E-03
Dermis	8.15E-07	8.04E-01	2.28E-02	1.68E-06	2.10E+00	5.11E-02	2.72E-06	4.79E-01	1.93E-02
Subcutis	5.10E-05	1.71E-01	7.67E-03	1.04E-04	4.81E-01	1.66E-02	1.69E-04	1.09E-01	6.21E-03
Fat	7.20E-05	5.69E-02	3.17E-03	1.46E-04	1.69E-01	6.33E-03	2.30E-04	4.03E-02	2.73E-03
Muscle	1.39E-06	7.09E-02	1.21E-02	3.94E-06	1.25E-01	1.44E-02	1.26E-06	4.44E-02	1.13E-02

**Table 3.** Current density of each skin layer for each electrode placement. Min = Minimum value; Max = Maximum value; Avg = Average value.

demonstrated no significant change in the average EF value at 1 mm from the center of the wound, group 1 and group 2 exhibited substantial increase in the average EF value at a wound diameter of 4 mm compared to 10 mm and 8 mm (Table 4).

### Discussions

This study performed both in-vivo experiments and simulations to explore how different electrode placements affect the EF and wound healing facilitated by ES.

ES is a treatment used to heal chronic and acute wounds, and wound healing can be accelerated by modulating the EF. Previous studies have reported that ES increases fibroblast proliferation and the expression of reparative factors in wound healing process<sup>44</sup>. Furthermore, the electric field generated by electrical stimulation governs the direction of cell migration and promotes cell migration, a phenomenon known as electrotaxis or galvanotaxis<sup>32</sup>. An EF that mimics the endogenous EF accelerates wound healing, whereas an EF with a vector opposite to the endogenous EF disrupts the cell migration directionality and impedes wound healing. This study aimed to explore the impact of electrode placement on EF and wound healing.

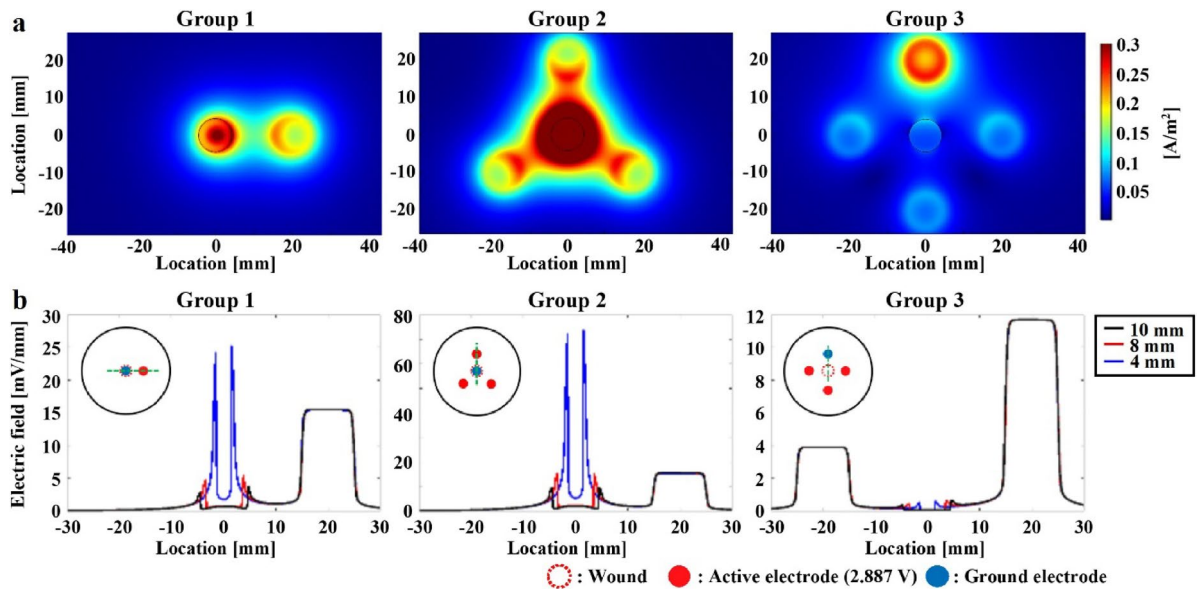


**Fig. 5.** Simulation analysis for each electrode placement. (a) Current density distribution across the section of the dermis when wound diameter is 10 mm. (b) Electric field distribution in the dermis across the wound and near the ground electrode when the wound diameter decreases from 10 to 4 mm. The green dotted line indicates the point from which the electrical field measurements were taken for each electrode placement.

Wound diameter	Electric field [mV/mm]		
	Group 1	Group 2	Group 3
10 mm	0.6331 ± 0.0018	1.8821 ± 0.0006	0.0438 ± 0.0004
8 mm	0.6699 ± 0.0019	1.9938 ± 0.0010	0.0480 ± 0.0006
4 mm	1.9131 ± 0.0291	5.5779 ± 0.0807	0.0547 ± 0.0005

**Table 4.** Average value of the EF in the wound center (ranging from -1 mm to 1 mm). The value in the table means average ± standard error of the mean.

In-vivo experiments have shown that the wound area ratio provides an intuitive measure of wound healing rate. As shown in the results, histological analysis indicated a reduction in the gap of epithelium and granulation tissue near the wound, signifying advanced re-epithelialization and remodeling<sup>56</sup>. A decreased gap of epithelium signifies re-epithelialization during the proliferation phase, and reduced gap of granulation tissue suggests transition from the proliferation phase to the remodeling phase<sup>57</sup>. The gaps of epithelium and granulation tissue (Fig. 4a–c) indicate that ES under the electrode placement of group 3 notably promotes re-epithelialization and remodeling, leading to the conclusion that this placement enables the most rapid wound healing. These findings suggest that electrode placement influences the efficacy of ES treatment and that placing four electrodes around the wound is optimal for accelerating re-epithelialization, remodeling, and overall wound healing.

The results of simulation indicate the formation of the EF by each electrode placement. Group 1 and group 2 exhibited high current densities at the edges of the wound and electrodes. Additionally, both group 1 and group 2 displayed a higher EF strength at the wound center compared to group 3 (Table 4). The peak in EF strength is likely due to a change in the medium at the edges of the electrodes and the wound. Moreover, the current density and electric field strength increase at the wound edge and center as the wound size decreases (Fig. 5a and b). A higher EF strength at the wound center in group 1 and group 2, compared to the surrounding normal skin, may impede wound healing. The stronger EF at the wound center, relative to periphery as wound size diminishes, may generate an EF vector opposing the endogenous EF. These opposing vectors and EF strength gradients obstruct cell migration<sup>32</sup>. To facilitate correct cell migration direction, it is beneficial to maintain gradient of electric field strength at the wound center with a differential in EF strength from the periphery, as demonstrated in group 2 (Fig. 5b). Moreover, simulation outcomes for group 1 and group 2 could lead to current overloading and heat generation. Reports indicate that increased temperature and heat generation adversely wound healing cutaneous vasoconstrictor responses, increasing oxidative stress, and reducing wound healing rates<sup>58–60</sup>. In simulations of a 4 mm diameter wound, the EF strength average at ± 0.5 mm from the wound edge of group 1 (13.9774 mV/mm) and group 2 (39.5161 mV/mm) is about 42.42 and 119.93 times higher, respectively than in group 3 (0.3295 mV/mm). EF strength can be converted to current density and heat generation using Ohm's law (Eq. 3), where  $J$  is current density,  $\sigma$  is electrical conductivity, and  $E$  is electric field, and Joule's law (Eq. 4), where  $Q$  is heat,  $I$  is current,  $R$  is resistance, and  $t$  is period. The current used in Eq. 4 of this study was derived from the RMS voltage.

A qualitative evaluation of relative thermal risk can be performed by translating electric field strength into the resulting heat generation. Heat generation at the wound edge of group 1 (2 mJ) and group 2 (15.7 mJ) exhibited increases by factors of 2,000 and 15,700 respectively, compared to group 3 (0.001 mJ). Elevated heat generation is associated with an increased thermal risk. These findings imply that placing electrodes over a wound may disrupt wound healing by causing disorientation in cell migration and heat generation.

$$J = \sigma E \quad (3)$$

$$Q = I^2 R t \quad (4)$$

There have also been documented skin burns resulting from the application of transcranial direct current stimulation (tDCS), which administers electrical stimulation through the skin<sup>61,62</sup>. Skin burns arise when electrodes are placed on uneven skin layers during tDCS application, leading to a locally excessive increase in current density around the sweat glands<sup>63</sup>. In in-vivo experiments, researchers observed an uneven wound surface and a complex composition of blood, fat, and muscle, while simulations confirmed the excessively increased current in both group 1 and group 2. These reports indicate that placing electrodes over wounds may negatively affect wound healing.

A notable finding from this study is that the electrode placements employed in previous studies had limitations, and this study proposes an alternative. Prior simulation studies revealed that the optimal placements consisted of covering the wounded area with the ground electrode and the entire intact skin with the active electrode<sup>48</sup>. This ring type configuration was commonly employed in the development of electric stimulation wound dressings<sup>13,64</sup>. However, in addition to the geometrical limitation whereby it cannot be applied to wounds of varying sizes and shape, the ring type also poses a risk of the heat and excessive current generation at on the wound.

This study has several limitations. First, the electrical stimulation used in the in-vivo experiments may not be identical to that simulated in the computational model. In our simulation, the effects of electrical stimulation on the electric field and current density were assessed using the root mean square voltage ( $V_{rms}$ ), which was set to match the power of the stimulation waveform used in the in-vivo experiments. Although  $V_{rms}$  ensures equivalent power delivery, discrepancies in the actual current between the simulation and in-vivo settings may still arise. These differences may be further attributed to variations in electrode structure and material properties (e.g., conductivity). Therefore, due to these potential discrepancies, the stimulation conditions in the simulation may not fully replicate the experimental scenario. As a result, the simulation results were interpreted qualitatively based on relative comparisons among experimental groups, rather than on absolute values. Future work should aim to reduce the discrepancy between simulation and experimental conditions by incorporating time-domain or Fourier finite element methods capable of representing pulsed waveforms, as well as by using material properties measured directly under in-vivo conditions. Second, the influence of electrochemical effects was not considered. The application of high-amplitude electrical stimulation can induce electrochemical nonlinear effects. Since our study focused solely on electrode placement, electrochemical effects were excluded from both the in-vivo and simulations. Due to discrepancies between the simulations and real biological conditions, we refrained from performing a quantitative analysis based on the simulation results and reported only qualitative evaluations. Direct measurement of current waveforms could help reveal potential nonlinear effects and provide further insight into how electrochemical reactions might influence wound healing. Such experimental investigations would complement the current findings and contribute to a deeper understanding of interactions in electrical stimulation for wound healing. Considering electrochemical effects and aligning the simulation environment more closely with real biological conditions to optimize wound healing treatment would be an interesting and valuable research. Third, there is a limitation concerning heat generation induced by electrical stimulation. In this study, we discussed the potential risk of heat generation among groups by comparing the relative heat generation derived from Eqs. (3) and (4). However, in actual in-vivo environments, various physiological factors—such as the degree of electrode–skin contact, cell migration, bleeding at the wound site, and inflammatory responses—can influence heat generation. These factors result in discrepancies between the calculated or simulated predictions and the actual heat generation. The heat generation reported in this study was calculated using a basic equation under highly limited conditions and should therefore be interpreted with caution. Therefore, systematic follow-up studies are necessary to investigate the impact of heat generation on wound healing under realistic physiological conditions.

In conclusion, this study suggests that increasing the number of electrodes, without placing them over the wound, can most effectively accelerate wound healing by upregulating the re-epithelialization and remodeling phases. This multi-integrative study presents a preclinical placement strategy to mitigate risks, emphasizing the necessity to optimize ES treatments and demonstrating significant potential for improving the clinic strategy.

### Data availability

The datasets generated during and/or analyzed during the current study are available from the corresponding author on reasonable request.

Received: 28 March 2025; Accepted: 27 October 2025

Published online: 07 November 2025

### References

1. Rabbani, M., Rahman, E., Powner, M. B. & Triantis, I. F. Making sense of electrical stimulation: a meta-analysis for wound healing. *Ann. Biomed. Eng.* **52**, 153–177 (2024).

2. Richardson, M. Acute wounds: an overview of the physiological healing process. *Nurs. Times* **100**, 50–53 (2004).
3. George Broughton, I., Janis, J. E. & Attinger, C. E. The basic science of wound healing. *Plastic Reconstr. Surg.* **117**, 12S–34S (2006).
4. Wallace, H. A., Basehore, B. M. & Zito, P. M. Wound healing phases. (2017).
5. Velnar, T., Bailey, T. & Smrkolj, V. The wound healing process: An overview of the cellular and molecular mechanisms. *J. Int. Med. Res.* **37**, 1528–1542 (2009).
6. Mustoe, T. A., O’Shaughnessy, K. & Kloeters, O. Chronic wound pathogenesis and current treatment strategies: A unifying hypothesis. *Plast. Reconstr. Surg.* **117**, 35S–41S (2006).
7. Khalil, H., Cullen, M., Chambers, H., Carroll, M. & Walker, J. Elements affecting wound healing time: An evidence based analysis. *Wound Repair Regen.* **23**, 550–556 (2015).
8. Werdin, F., Tenenhaus, M. & Rennekampff, H.-O. Chronic wound care. *Lancet* **372**, 1860–1862 (2008).
9. Sen, C. K. et al. Human skin wounds: a major and snowballing threat to public health and the economy. *Wound Repair Regen.* **17**, 763–771 (2009).
10. Leaper, D., Assadian, O. & Edmiston, C. E. Approach to chronic wound infections. *Br. J. Dermatol.* **173**, 351–358 (2015).
11. Moulik, P. K., Mtonga, R. & Gill, G. V. Amputation and mortality in new-onset diabetic foot ulcers stratified by etiology. *Diabetes Care* **26**, 491–494 (2003).
12. Ovington, L. G. Advances in wound dressings. *Clin. Dermatol.* **25**, 33–38 (2007).
13. Song, J. W. et al. Bioresorbable, wireless, and battery-free system for electrotherapy and impedance sensing at wound sites. *Sci. Adv.* **9**, eade4687 (2023).
14. Ngo, O. et al. Development of low frequency (20–100 kHz) clinically viable ultrasound applicator for chronic wound treatment. *IEEE Trans. Ultrason. Ferroelectr. Freq. Control* **66**, 572–580 (2018).
15. Wang, X., Zhang, W., Zhou, Q. & Ran, F. Integrating supercapacitor with sodium hyaluronate based hydrogel as a novel all-in-one wound dressing: Self-powered electronic stimulation. *Chem. Eng. J.* **452**, 139491 (2023).
16. Xu, J. et al. Non-contact electrical stimulation as an effective means to promote wound healing. *Bioelectrochemistry* **146**, 108108 (2022).
17. Yadav, A. & Gupta, A. Noninvasive red and near-infrared wavelength-induced photobiomodulation: Promoting impaired cutaneous wound healing. *Photodermatol. Photoimmunol. Photomed.* **33**, 4–13 (2017).
18. Nourian Dehkordi, A., Mirahmadi Babaheydari, F., Chehelgerdi, M. & Raeisi Dehkordi, S. Skin tissue engineering: Wound healing based on stem-cell-based therapeutic strategies. *Stem Cell Res. Therapy* **10**, 1–20 (2019).
19. Thackham, J. A., McElwain, D. S. & Long, R. J. The use of hyperbaric oxygen therapy to treat chronic wounds: A review. *Wound Repair Regen.* **16**, 321–330 (2008).
20. Cox, A. & Bousfield, C. Velcro compression wraps as an alternative form of compression therapy for venous leg ulcers: A review. *Br. J. Community Nurs.* **26**, S10–S20 (2021).
21. Farahani, M. & Shafiee, A. Wound healing: from passive to smart dressings. *Adv. Healthcare Mater.* **10**, 2100477 (2021).
22. del Pozo, J. L. et al. Effect of electrical current on the activities of antimicrobial agents against *Pseudomonas aeruginosa*, *Staphylococcus aureus*, and *Staphylococcus epidermidis* biofilms. *Antimicrob. Agents Chemother.* **53**, 35–40. <https://doi.org/10.1128/AAC.00237-08> (2009).
23. Santamato, A. et al. Effectiveness of the frequency rhythmic electrical modulation system for the treatment of chronic and painful venous leg ulcers in older adults. *Rejuvenation Res* **15**, 281–287. <https://doi.org/10.1089/rej.2011.1236> (2012).
24. Peters, E. J., Lavery, L. A., Armstrong, D. G. & Fleischli, J. G. Electric stimulation as an adjunct to heal diabetic foot ulcers: A randomized clinical trial. *Arch. Phys. Med. Rehabil.* **82**, 721–725. <https://doi.org/10.1053/apmr.2001.23780> (2001).
25. Snyder, S., DeJulius, C. & Willits, R. K. Electrical stimulation increases random migration of human dermal fibroblasts. *Ann. Biomed. Eng.* **45**, 2049–2060. <https://doi.org/10.1007/s10439-017-1849-x> (2017).
26. Franek, A. et al. Using high-voltage electrical stimulation in the treatment of recalcitrant pressure ulcers: Results of a randomized, controlled clinical study. *Ostomy Wound Manage.* **58**, 30–44 (2012).
27. Foulds, I. S. & Barker, A. T. Human skin battery potentials and their possible role in wound healing. *Br. J. Dermatol.* **109**, 515–522. <https://doi.org/10.1111/j.1365-2133.1983.tb07673.x> (1983).
28. Cheah, Y. J., Buyong, M. R. & Mohd Yunus, M. H. Wound healing with electrical stimulation technologies: A review. *Polymers* <https://doi.org/10.3390/polym13213790> (2021).
29. Reid, B. & Zhao, M. The electrical response to injury: Molecular mechanisms and wound healing. *Adv. Wound Care (New Rochelle)* **3**, 184–201. <https://doi.org/10.1089/wound.2013.0442> (2014).
30. Vieira, A. C. et al. Ionic components of electric current at rat corneal wounds. *PLoS ONE* **6**, e17411. <https://doi.org/10.1371/journal.pone.0017411> (2011).
31. Watsky, M. A. Nonselective cation channel activation during wound healing in the corneal endothelium. *Am J Physiol* **268**, C1179–1185. <https://doi.org/10.1152/ajpcell.1995.268.5.C1179> (1995).
32. Zhao, M. Electrical fields in wound healing—An overriding signal that directs cell migration. *Semin. Cell Dev. Biol.* **20**, 674–682. <https://doi.org/10.1016/j.semcdb.2008.12.009> (2009).
33. Messerli, M. A. & Graham, D. M. Extracellular electrical fields direct wound healing and regeneration. *Biol. Bull.* **221**, 79–92. <https://doi.org/10.1086/BBLv221n1p79> (2011).
34. Kai, H. et al. Accelerated wound healing on skin by electrical stimulation with a bioelectric plaster. *Adv. Healthcare Mater.* **6**, 1700465 (2017).
35. Lei, H. & Fan, D. Conductive, adaptive, multifunctional hydrogel combined with electrical stimulation for deep wound repair. *Chem. Eng. J.* **421**, 129578 (2021).
36. Wirsing, P. G., Habrom, A. D., Zehnder, T. M., Friedli, S. & Blatti, M. Wireless micro current stimulation—an innovative electrical stimulation method for the treatment of patients with leg and diabetic foot ulcers. *Int. Wound. J.* **12**, 693–698. <https://doi.org/10.1111/iwj.12204> (2015).
37. Ud-Din, S. & Bayat, A. Electrical stimulation and cutaneous wound healing: A review of clinical evidence. *Healthcare (Basel)* **2**, 445–467. <https://doi.org/10.3390/healthcare2040445> (2014).
38. Rajendran, S. B., Challen, K., Wright, K. L. & Hardy, J. G. Electrical stimulation to enhance wound healing. *J. Funct. Biomater.* <https://doi.org/10.3390/jfb12020040> (2021).
39. Gomez-Tames, J. D., Gonzalez, J. & Yu, W. A simulation study: Effect of the inter-electrode distance, electrode size and shape in transcutaneous electrical stimulation. *Ann. Int. Conf. IEEE Eng. Med. Biol. Soc.* **2012**, 3576–3579. <https://doi.org/10.1109/EMBC.2012.6346739> (2012).
40. Pfalzgraff, A., Brandenburg, K. & Weindl, G. Antimicrobial peptides and their therapeutic potential for bacterial skin infections and wounds. *Front. Pharmacol.* **9**, 281. <https://doi.org/10.3389/fphar.2018.00281> (2018).
41. Kloth, L. C. Electrical stimulation for wound healing: A review of evidence from in vitro studies, animal experiments, and clinical trials. *Int. J. Low Extrem. Wounds* **4**, 23–44. <https://doi.org/10.1177/1534734605275733> (2005).
42. Atalay, C. & Yilmaz, K. B. The effect of transcutaneous electrical nerve stimulation on postmastectomy skin flap necrosis. *Breast Cancer Res. Treat* **117**, 611–614. <https://doi.org/10.1007/s10549-009-0335-z> (2009).
43. Yang, S. M. et al. Soft, wireless electronic dressing system for wound analysis and biophysical therapy. *Nano Today* **47**, 101685 (2022).

44. Gurgen, S. G., Sayin, O., Cetin, F. & Tuc Yucel, A. Transcutaneous electrical nerve stimulation (TENS) accelerates cutaneous wound healing and inhibits pro-inflammatory cytokines. *Inflammation* **37**, 775–784. <https://doi.org/10.1007/s10753-013-9796-7> (2014).
45. Borba, G. C., Hochman, B., Liebano, R. E., Enokihara, M. M. & Ferreira, L. M. Does preoperative electrical stimulation of the skin alter the healing process?. *J. Surg. Res.* **166**, 324–329. <https://doi.org/10.1016/j.jss.2009.08.018> (2011).
46. Franek, A. et al. Effect of high voltage monophasic stimulation on pressure ulcer healing: Results from a randomized controlled trial. *Wounds* **23**, 15–23 (2011).
47. Liang, Y. et al. Application of stable continuous external electric field promotes wound healing in pig wound model. *Bioelectrochemistry* **135**, 107578. <https://doi.org/10.1016/j.bioelechem.2020.107578> (2020).
48. Sun, Y. S. Electrical stimulation for wound-healing: Simulation on the effect of electrode configurations. *Biomed. Res. Int.* **2017**, 5289041. <https://doi.org/10.1155/2017/5289041> (2017).
49. Akhtari, N. et al. Natural agents as wound-healing promoters. *Inflammopharmacology* **32**, 101–125 (2024).
50. Ziroglu, N. et al. The antibiotics supplemented bone cement improved the masquelet's induced membrane in a rat femur critical size defect model. *Injury* **54**, 329–338 (2023).
51. Souza, A. K. et al. Effect of high voltage pulsed current on the integration of total skin grafts in rats submitted to nicotine action. *J. Tissue Viabil.* **28**, 161–166 (2019).
52. Seran, E., Godefroy, M., Pili, E., Michielsen, N. & Bondiguel, S. What we can learn from measurements of air electric conductivity in 222Rn-rich atmosphere. *Earth Space Sci.* **4**, 91–106. <https://doi.org/10.1002/2016ea000241> (2017).
53. Celik, N., Manivannan, N., Strudwick, A. & Balachandran, W. Graphene-enabled electrodes for electrocardiogram monitoring. *Nanomaterials* <https://doi.org/10.3390/nano6090156> (2016).
54. Frahm, K. S., Morch, C. D., Grill, W. M. & Andersen, O. K. Experimental and model-based analysis of differences in perception of cutaneous electrical stimulation across the sole of the foot. *Med. Biol. Eng. Comput.* **51**, 999–1009. <https://doi.org/10.1007/s11517-013-1079-9> (2013).
55. Seitz, S., Seemann, G. & Dossel, O. in *2008 Computers in cardiology*. 489–492 (IEEE).
56. Zhang, Z. et al. Effective electrical stimulation by a Poly (l-lactic acid)/Vitamin B2-Based piezoelectric generator promotes wound healing. *Eur. Polymer J.* **189**, 111962 (2023).
57. Abed, H. et al. Incidence and management of graft erosion, wound granulation, and dyspareunia following vaginal prolapse repair with graft materials: A systematic review. *Int. Urogynecol. J.* **22**, 789–798 (2011).
58. Chakraborty, U. & Pradhan, D. High temperature-induced oxidative stress in *Lens culinaris*, role of antioxidants and amelioration of stress by chemical pre-treatments. *J. Plant Interact.* **6**, 43–52. <https://doi.org/10.1080/17429145.2010.513484> (2011).
59. Pearson, J., Lucas, R. A. & Crandall, C. G. Elevated local skin temperature impairs cutaneous vasoconstrictor responses to a simulated haemorrhagic challenge while heat stressed. *Exp. Physiol.* **98**, 444–450. <https://doi.org/10.1113/expphysiol.2012.068353> (2013).
60. Zhang, Q. et al. Daytime radiative cooling dressings for accelerating wound healing under sunlight. *Nature Chem. Eng.* **1**, 301–310. <https://doi.org/10.1038/s44286-024-00050-4> (2024).
61. Palm, U. et al. Skin lesions after treatment with transcranial direct current stimulation (tDCS). *Brain Stimul.* **1**, 386–387. <https://doi.org/10.1016/j.brs.2008.04.003> (2008).
62. Matsumoto, H. & Ugawa, Y. Adverse events of tDCS and tACS: A review. *Clin. Neurophysiol. Pract.* **2**, 19–25. <https://doi.org/10.1016/j.cnp.2016.12.003> (2017).
63. Loo, C. K. et al. Avoiding skin burns with transcranial direct current stimulation: Preliminary considerations. *Int. J. Neuropsychopharmacol.* **14**, 425–426. <https://doi.org/10.1017/S1461145710001197> (2011).
64. Wang, X. F. et al. Flexible electrical stimulation device with Chitosan-Vaseline(R) dressing accelerates wound healing in diabetes. *Bioact. Mater.* **6**, 230–243. <https://doi.org/10.1016/j.bioactmat.2020.08.003> (2021).

## Acknowledgements

This work was supported by the National Research Foundation of Korea (NRF) grant funded by the Korean government (MSIT) (RS-2022-NR070502 and RS-2024-00333219). This work was supported by Soonchunhyang University.

## Author contributions

Conceptualization, S.K. and D.K.; Methodology, S.K., D.K., and Y.C.; Validation, S.K. and D.K.; Formal Analysis, S.K., D.K., E.K., J.S.L., and J.Y.L.; Investigation, S.K. and D.K.; Resources, S.K., D.K., and Y.C.; Data Curation, S.K. and D.K.; Writing—Original Draft, S.K. and D.K.; Writing—Review and Editing, E.K. and J.S.L.; Visualization, S.K. and D.K.; Supervision, E.K.; Project Administration, E.K.; Funding Acquisition, E.K. and I.Y.K.

## Declarations

## Competing interests

The authors declare no competing interests.

## Additional information

**Supplementary Information** The online version contains supplementary material available at <https://doi.org/10.1038/s41598-025-26070-5>.

**Correspondence** and requests for materials should be addressed to I.Y.K. or E.P.

**Reprints and permissions information** is available at [www.nature.com/reprints](http://www.nature.com/reprints).

**Publisher's note** Springer Nature remains neutral with regard to jurisdictional claims in published maps and institutional affiliations.

**Open Access** This article is licensed under a Creative Commons Attribution-NonCommercial-NoDerivatives 4.0 International License, which permits any non-commercial use, sharing, distribution and reproduction in any medium or format, as long as you give appropriate credit to the original author(s) and the source, provide a link to the Creative Commons licence, and indicate if you modified the licensed material. You do not have permission under this licence to share adapted material derived from this article or parts of it. The images or other third party material in this article are included in the article's Creative Commons licence, unless indicated otherwise in a credit line to the material. If material is not included in the article's Creative Commons licence and your intended use is not permitted by statutory regulation or exceeds the permitted use, you will need to obtain permission directly from the copyright holder. To view a copy of this licence, visit <http://creativecommons.org/licenses/by-nc-nd/4.0/>.

© The Author(s) 2025